SINTEF
PROCEEDINGS 6

14th International Conference on CFD in
Oil & Gas, Metallurgical and Process Industries
SINTEF, Trondheim, Norway, October 12–14, 2020

Proceedings from the 14th International Conference on CFD in Oil & Gas, Metallurgical and Process Industries

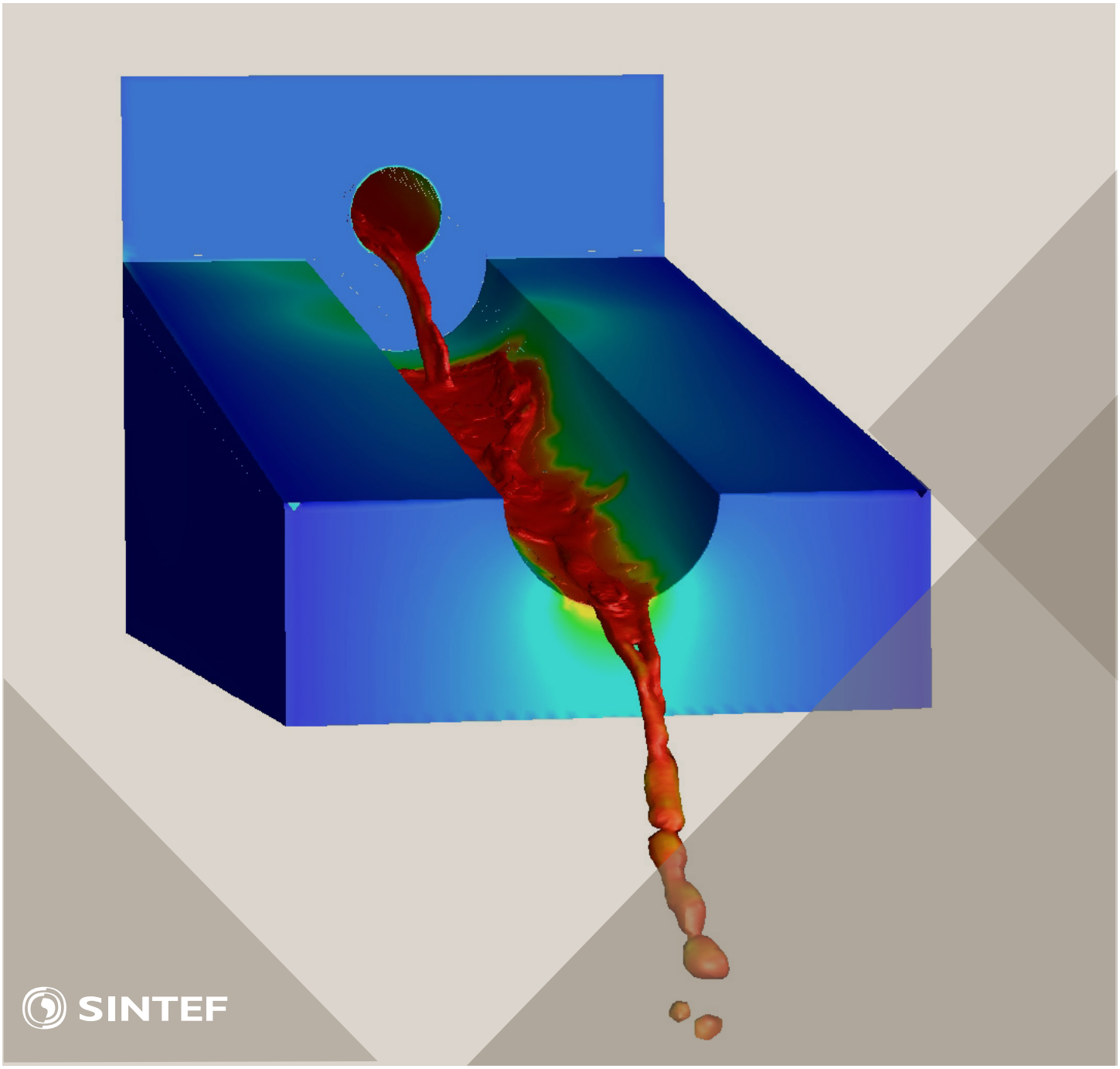

SINTEF Proceedings

Editors:
Jan Erik Olsen, Jan Hendrik Cloete and Stein Tore Johansen

Proceedings from the 14th International Conference on CFD in Oil & Gas, Metallurgical and Process Industries

SINTEF, Trondheim, Norway
October 12–14, 2020

SINTEF Academic Press

SINTEF Proceedings 6
Editors: Jan Erik Olsen, Jan Hendrik Cloete and Stein Tore Johansen

Proceedings from the 14th International Conference on CFD in Oil & Gas, Metallurgical and Process Industries, SINTEF, Trondheim, Norway, October 12–14, 2020

Keywords:
CFD, fluid dynamics, modelling

Cover illustration: Tapping of metal by Jan Erik Olsen

ISSN 2387-4295 (online)
ISBN 978-82-536-1684-1 (pdf)

SINTEF Academic Press
Address: Børrestuveien 3
PO Box 124 Blindern
N-0314 OSLO
Tel: +47 40 00 51 00

www.sintef.no/community
www.sintefbok.no

14th International Conference on CFD In Oil & Gas, Metallurgical and Process Industries
SINTEF, Trondheim, NORWAY
October 12-14, 2020

INVERSE MODELLING OF INTERFACIAL TENSION BETWEEN FERROALLOY AND SLAG USING OPENFOAM

Sergey BUBLIK[1*], **Kristian Etienne EINARSRUD**[1†]
[1]Department of Materials Science and Engineering, Norwegian University of Science and Technology (NTNU), Trondheim, NORWAY

[*] E-mail: sergey.bublik@ntnu.no
[†] E-mail: kristian.e.einarsrud@ntnu.no

ABSTRACT

The entrainment of molten ferroalloy droplets in slag during tapping operations is strongly related to turbulence and interfacial forces between alloy and slag. Therefore, interfacial phenomena are of great importance for the ferroalloys industry and a better understanding of entrainment mechanisms can reduce ferroalloy losses with slag flow. The interfacial tension plays an important role in the interaction between ferroalloy and slag due to the ability to modify droplets shape and the flow regime. However, the measurement of interfacial tension between two molten phases is challenging due to high temperatures and complex composition. In particular, surface active elements significantly influence the interfacial tension. Available methods for determining the interfacial tension are often based on using complex equipment (e.g. a furnace equipped with an X-ray camera) and tend to have significant uncertainty in measurements. In this study, a methodology for inverse modelling of interfacial tension between ferroalloys and slag was developed and investigated by combining experimental measurements, reduced order modelling and simulations in OpenFOAM. The proposed method relies upon experimental determination of the shape of single droplets, from which surface tension can be determined using numerical procedures such as elliptic fitting and the low-bond axisymmetric drop shape technique. Given relevant material properties for single phases, parameters governing the interactions between the phases, e.g. interfacial tension, can be determined by comparing parametric simulations to experiments in which interactions are present. Simulations are realized using multiphaseInterFoam for a slag droplet at rest on molten metal in an inert atmosphere. The current work describes the modelling strategy and demonstrates its applicability to recent experiments for the FeMn-slag system. The uncertainty and sensibility of the method are assessed by comparing different available simulation settings, resolution and the uncertainty in the experimental data.

Keywords: Inverse modelling, interfacial phenomena, interfacial tension, slag metal separation.

NOMENCLATURE

Greek Symbols

α	Phase fraction within the range $0 < \alpha < 1$.
γ	Surface or interfacial tension, $[N/m]$.
θ	Contact angle, [°].
μ	Dynamic viscosity, $[Pa \cdot s]$.
ν	Kinematic viscosity, $[m^2/s]$.
ρ	Density, $[kg/m^3]$.
$\Delta\rho$	Density difference between two phases, $[kg/m^3]$.

Latin Symbols

a	Length of the semi-major axis of an ellipse, $[m]$.
b	Length of the semi-minor axis of an ellipse, $[m]$.
c	Capillary constant, $[m^{-2}]$.
g	Gravitational acceleration, 9,81, $[m/s^2]$.
h	Height, $[m]$.
m	Weight, $[kg]$.
P	Pressure, $[Pa]$.
ΔP	Pressure difference across the interface, $[Pa]$.
ΔP_0	Pressure difference at a reference plane, $[Pa]$.
R_0	Radius of curvature at the droplet apex, $[m]$.
R_1, R_2	Principal radii of curvature, $[m]$.
U	Fluid velocity, $[m/s]$.
U_r	Compression velocity, $[m/s]$.
V	Volume, $[m^3]$.
x	Position vector, $[m]$.

Sub/superscripts

n	Phase.
exp	Corresponding to experiments.
sim	Corresponding to simulations.
vis	Visible.
$non-vis$	Non-visible.
$slag$	Corresponding to slag.
$FeMn$	Corresponding to FeMn.
Ar	Corresponding to argon atmosphere.
$slag-Ar$	Interface between slag and Ar.
$FeMn-Ar$	Interface between FeMn and Ar.
$FeMn-slag$	Interface between FeMn and slag.

INTRODUCTION

Ferroalloys are widely used to improve various properties of steels and alloys, for example, hardness, ductility and corrosion resistance (Holappa, 2013). Ferroalloys are produced mainly by carbothermic reduction in submerged arc furnaces (SAFs), where raw materials are heated up by applying the electric current to electrodes. Raw materials in the production of ferroalloys are complex in chemical composition and therefore all other elements, which do not end up in the alloy phase, need to be separated from the alloy and removed as the

slag. The removal of molten material (a mixture of slag and alloy) is carried out through an operation which is called tapping. During this operation, the SAF is opened by a drilling machine and thereafter the molten material comes out from the furnace into a cascade of ladles (Tangstad, 2013). The first ladle in the cascade is used for separation of slag and alloy due to the density differences, and storing the alloy, while the following ladles are used only for the slag (Fig. 1). The molten flow typically disintegrates after the impact with either the surface of the alloy ladle or the molten material due to turbulence and interfacial forces between alloy and slag (Lee, 2016). It results in the formation and entrainment of small alloy droplets in slag phase, which then overflows to slag ladles, contributing to the alloy losses. For this reason, the interfacial phenomena are vital for the ferroalloys industry and a better understanding of entrainment mechanisms can reduce ferroalloy losses with slag flow.

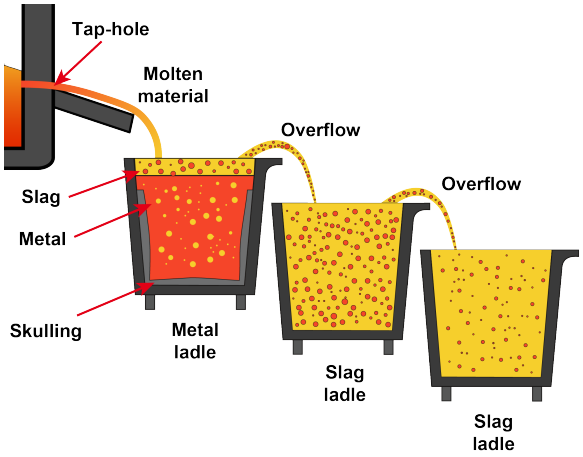

Figure 1: Tapping of the SAF.

The interfacial tension characterizes the interaction between slag and metal and the stability of the interface between slag and alloy (Ooi *et al.*, 1974). High interfacial tension results in better separation, while its lower values promote the formation of slag-metal emulsion. Furthermore, surface active elements, which can significantly reduce the interfacial tension, are typically present in molten systems (Li *et al.*, 2003). In ferroalloys production, the surface active elements are represented by sulphur and oxygen. The thermodynamic equilibrium between alloy and slag is described by the reaction (Saridikmen *et al.*, 2007):

$$[S] + (O^{2-}) \Leftrightarrow (S^{2-}) + [O], \tag{1}$$

where $[S], [O]$ are sulphur and oxygen in alloy, $(S^{2-}), (O^{2-})$ are sulphur and oxygen in slag.

In addition, the interfacial tension can affect the terminal (settling) velocity of alloy droplets in slag phase. Droplets can have various regimes (Clift *et al.*, 1978), which are based on physical properties such as density, interfacial tension and viscosity. Hence, depending on the regime, the surface area of a droplet can be significantly different from its initial shape, meaning that the drag force which acts in the flow direction will also be affected by the regime.

Experimentally, surface and interfacial tension between two molten materials are determined by melting materials in a furnace equipped with an X-ray camera (Jakobsson *et al.*, 2000) or by applying the sessile drop technique with a digital camera (Kim *et al.*, 2010). After recording images from interfacial interaction between two different phases and a gas, surface or interfacial tension are obtained by the numerical solution of the Young-Laplace equation. However, in most cases, the measurement of interfacial/surface tension is extremely complicated due to high temperatures and complex composition of materials.

The equilibrium in the three-fluid interaction is described schematically as shown in Fig. 2a and consequently the surface and interfacial tension vectors are characterized by applying the Neumann vectorial triangle (Fig. 2b). At the equilibrium the sum of surface forces equals to zero, therefore the force balance for all interfaces ($\alpha\beta$, $\alpha\delta$, $\beta\delta$) is written as (Rowlinson and Widom, 2002):

$$\begin{aligned} \gamma_{\alpha\beta} + \gamma_{\beta\delta}\cos\beta + \gamma_{\alpha\delta}\cos\alpha &= 0 \\ \gamma_{\alpha\beta}\cos\beta + \gamma_{\beta\delta} + \gamma_{\alpha\delta}\cos\delta &= 0 \\ \gamma_{\alpha\beta}\cos\alpha + \gamma_{\beta\delta}\cos\delta + \gamma_{\alpha\delta} &= 0, \end{aligned} \tag{2}$$

where $\gamma_{\alpha\beta}$, $\gamma_{\alpha\delta}$, $\gamma_{\beta\delta}$ is the tension of the $\alpha\beta$, $\alpha\delta$, $\beta\delta$ interface, respectively.

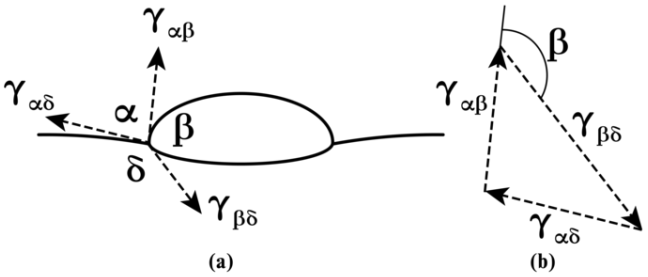

Figure 2: (a) The equilibrium between a fluid droplet, resting on the interface between two fluids of different densities, (b) the Neumann's triangle; $\gamma_{\alpha\beta}$ corresponds to surface tension between slag and gas, $\gamma_{\alpha\delta}$ corresponds to surface tension between FeMn alloy and gas, $\gamma_{\beta\delta}$ corresponds to interfacial tension between FeMn alloy and slag.

Based on the law of cosines, the force balance can be rewritten in order to obtain a numerical value of $\cos\beta$:

$$\cos\beta = \frac{\gamma_{\alpha\delta}^2 - \gamma_{\alpha\beta}^2 - \gamma_{\beta\delta}^2}{2\gamma_{\alpha\beta}\gamma_{\beta\delta}}. \tag{3}$$

A methodology allowing for the observations of interfacial flow between ferromanganese alloys (FeMn) and slag, was developed by the authors (Bublik *et al.*, 2019), based on experiments using a sessile drop furnace and recording of images.

In this work, the interfacial tension between FeMn alloy and slag has been determined based on a new inverse modelling strategy, combining simulations with analysis of images from the sessile drop furnace. The model applicability and sensibility has been studied and discussed by comparing different settings in OpenFOAM and the uncertainty in experimental data.

METHOD DESCRIPTION

A. Materials preparation

The synthetic FeMn alloy and slag for experiments in the sessile drop furnace were prepared from pure powders according to the industrial composition (Table 1). The powders were mixed and melted separately in a graphite crucible in an induction furnace in Ar atmosphere at 1773 K, 60 min of holding for FeMn and 5 min of holding for slag. After the first melting, both FeMn and slag were removed from

the crucible, ground into small pieces in a ball mill and then remelted in the graphite crucible in the induction furnace at the same operational parameters.

Table 1: Chemical composition of materials used for the experiments in the sessile drop furnace.

Material	Chemical composition, wt. %							
	Mn	**Fe**	**C**	**MnO**	**CaO**	**MgO**	**SiO_2**	**Al_2O_3**
HC FeMn	78	15	7	-	-	-	-	-
FeMn slag	-	-	-	38	23	6	23	10

B. Experimental setup

The sessile drop technique was applied in order to determine surface tension of alloy/slag and to investigate the interfacial behaviour between FeMn and slag:

- In experiments, where *surface tension* was measured, a piece of slag or FeMn alloy was placed on a graphite substrate (ISO-88) as shown in Fig. 3 and Fig. 4, the furnace is heated up and images of interaction between slag-graphite or alloy-graphite were recorded. Thereafter, the images were analyzed by means of the Young-Laplace equation.

- In experiments for measurement of *interfacial interaction*, small FeMn pieces were placed in a graphite cup (Fig. 5) and a slag piece was placed on top of the FeMn layer. Subsequently, the interfacial tension is measured by inverse modelling in OpenFOAM.

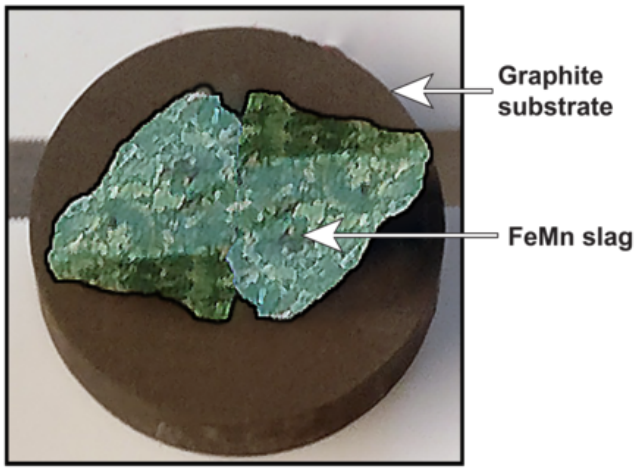

Figure 3: Slag on a graphite substrate before experiments for measurement of surface tension in the sessile drop furnace.

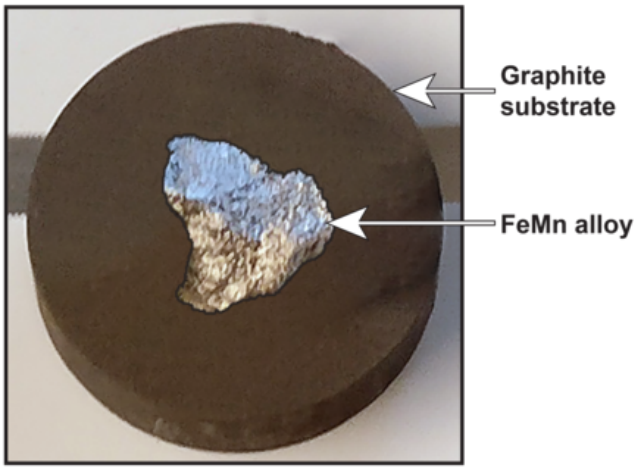

Figure 4: FeMn alloy on a graphite substrate before experiments for measurement of surface tension in the sessile drop furnace.

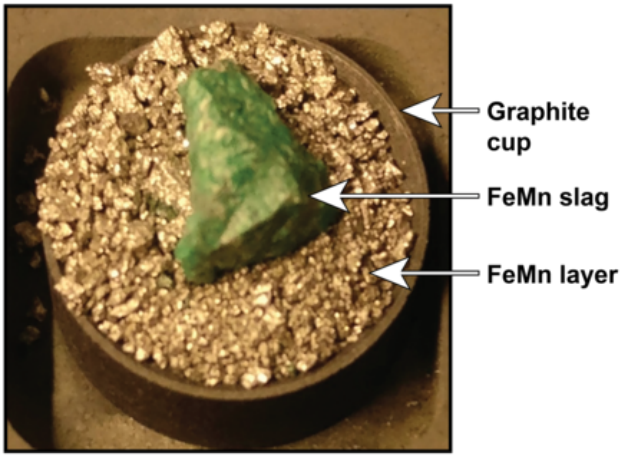

Figure 5: Slag on top of FeMn pieces in a graphite cup before experiments for measurement of interfacial tension in the sessile drop furnace.

The sessile drop furnace (Fig. 6) was equipped with a digital video camera (Sony XCD-SX910CR, Sony Corporation, Millersville, MD) with a telecentric lens (Navitar 1-50993D) to record images from the molten samples with the resolution of 1280x1024 pixels. The experiments were done at the maximum temperature of 1623, 1673, 1723 K and holding time of 5, 10, 15 min.

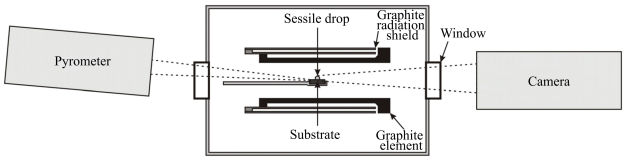

Figure 6: Schematic illustration of the sessile drop furnace.

C. Methodology for inverse modelling

The methods consist of the followings steps:

a) Conduct experiments with a single slag or FeMn alloy droplet and determine the *surface tension* of each phase.

b) Conduct experiments in the sessile drop furnace with FeMn layer and a slag piece on top.

c) Conduct simulations in OpenFOAM for a certain range of interfacial tension using densities of FeMn alloy and slag in the molten state, weight of the slag droplet and surface tensions determined from step *a)*.

d) Calculate visible (or non-visible) height of the slag droplet (in %) both for experiments and simulations. Compare experimental and simulation values to determine *interfacial tension*.

Determination of surface tension

The Young-Laplace equation describes the relationship between the curvature of a droplet and surface tension:

$$\Delta P = \gamma\left(\frac{1}{R_1} + \frac{1}{R_2}\right). \tag{4}$$

If external forces are not applied on a droplet, except of the gravity, the pressure difference is expressed as:

$$\begin{aligned}\Delta P &= \Delta P_0 + \Delta\rho g h \\ &= \frac{2\gamma}{R_0} + \Delta\rho g h.\end{aligned} \tag{5}$$

a) Surface tension of slag is determined by the elliptic solution of the Young-Laplace equation (Hernandez-Baltazar and Gracia-Fadrique, 2005), implemented in MATLAB. Surface tension (in N/m) is determined from the expression:

$$\gamma = \frac{a^2(\rho_{slag} - \rho_{Ar})g}{\frac{a^3}{b^3} + \frac{a}{b} - 2}, \tag{6}$$

where the values of the semi-major axis a and the semi-minor axis b are obtained from image analysis of slag droplets in experiments, after fitting an ellipse to the slag curvature (Fig. 7). The elliptic solution fails if contact angle (θ) between the droplet and the substrate is lower than 90°, giving wrong values for surface tension. In addition, there is a significant uncertainty in measurements by this method if droplet's surface during experiments is rough.

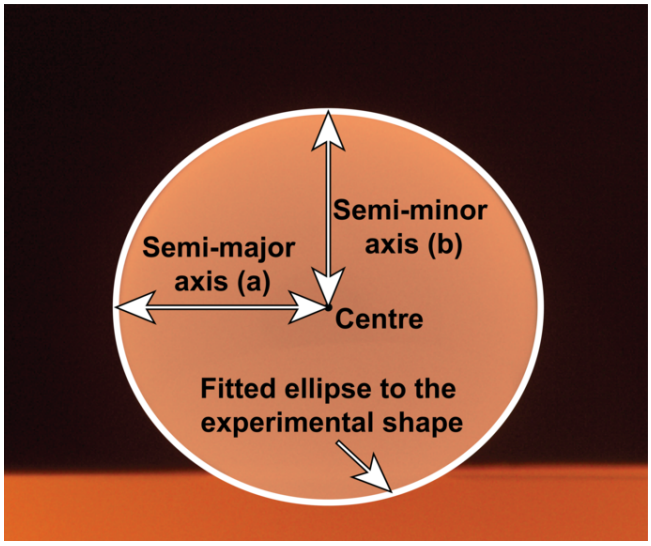

Figure 7: Ellipsoidal fitting to the slag droplet during experiments in the sessile drop furnace.

b) The contact angle between FeMn alloy and the graphite substrate is lower than 90°, and the surface roughness is high (Fig. 8). For this reason, surface tension of FeMn alloy is measured by a plugin for ImageJ (Rueden *et al.*, 2017), which is based on the low-bond axisymmetric drop shape analysis (LBADSA) (Stalder *et al.*, 2010). The plugin extracts parameters of droplet's contour after the fitting of the Young-Laplace equation to the image data (Fig. 9). The output from the plugin is the capillary constant c, which is related to surface tension of FeMn (γ) through the equation:

$$c = \frac{(\rho_{FeMn} - \rho_{Ar})g}{\gamma}. \tag{7}$$

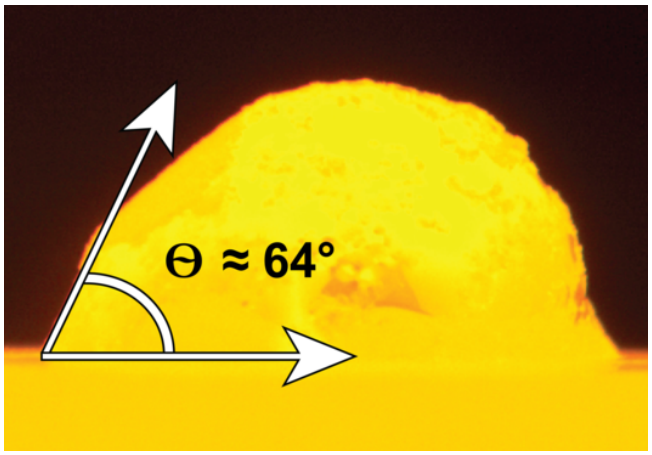

Figure 8: FeMn alloy surface during experiments in the sessile drop furnace.

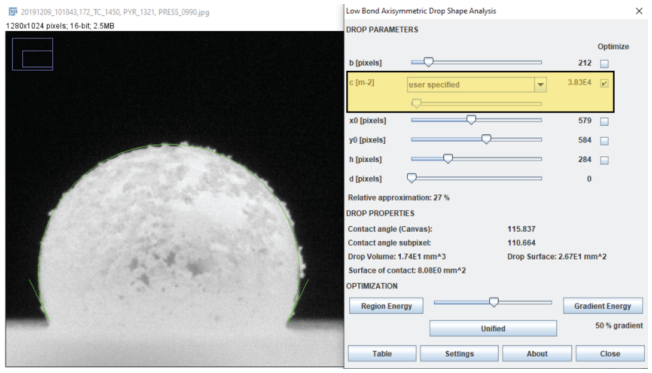

Figure 9: Fitting and measurement of parameters of a FeMn droplet from the image data by LBADSA plugin for ImageJ.

Simulations using multiphaseInterFoam

Simulations were carried out in OpenFOAM 6 (Weller *et al.*, 1998) using *multiphaseInterFoam*, a solver for N incompressible fluids which captures the interfaces and includes surface tension and contact angle effect for each phase, with optional mesh motion and topology changes.
multiphaseInterFoam is based on the volume-of-fluid (VOF) method (Hirt and Nichols, 1981), where a transport equation is applied to define the volume fraction α_n of each of the phases (Andersson, 2010). The transport equation is solved with the continuity and momentum equation for each phase (Damian, 2012). The continuity equation is defined as:

$$\nabla \cdot \mathbf{U} = 0. \tag{8}$$

The transport equation for α is:

$$\frac{\partial \alpha}{\partial t} + \nabla \cdot (\mathbf{U}\alpha) + \nabla \cdot [\mathbf{U}_r \alpha(1-\alpha)] = 0, \tag{9}$$

and the momentum equation is expressed as:

$$\frac{\partial(\rho \mathbf{U})}{\partial t} + \nabla \cdot (\rho \mathbf{U}\mathbf{U}) = -\nabla p + \mathbf{g} \cdot \mathbf{x} \nabla \rho + \mu \left[\nabla \mathbf{U} + (\nabla \mathbf{U})^T\right] + \gamma \kappa \nabla \alpha, \tag{10}$$

where $\mu \left[\nabla \mathbf{U} + (\nabla \mathbf{U})^T\right]$ is the viscous term, $\gamma\kappa\nabla\alpha$ is surface tension force per unit volume, which is based on the continuum surface force model (Berberovic *et al.*, 2009), κ is the mean curvature of the free surface:

$$\kappa = -\nabla \cdot \left(\frac{\nabla \alpha}{|\nabla \alpha|}\right). \tag{11}$$

The mixture density (ρ) and viscosity (μ) are calculated as weighted averages based on the phase fraction in a control volume, i.e.:

$$\rho = \sum_n \rho_n \alpha_n \tag{12}$$

and

$$\mu = \sum_n \mu_n \alpha_n. \tag{13}$$

Evidently, cells with only a single phase, retain the material properties of the phase in question.

Reduced order modelling

In order to determine the interfacial tension between slag and alloy, the non-visible height of droplets (in %) both in experiments and simulations was calculated by the following procedure:

A. Procedure for slag droplets in experiments

1. Measure the weight of the slag droplet before experiments, m_{slag}.

2. Calculate the (total) volume of the slag droplet in molten state, V_{total}^{slag}:

$$V_{total}^{slag} = \frac{m_{slag}}{\rho_{slag}}. \tag{14}$$

3. The slag droplet resting on top of the FeMn layer is assumed to be a spherical cap both above and below the FeMn-Ar interface as shown in Fig. 10. According to the geometric properties of the spherical cap, a and h_{vis}^{exp} can be obtained directly by measuring corresponding distances, while the height below the interface, $h_{non-vis}^{exp}$, is unknown, and therefore it has to be determined via additional calculations.

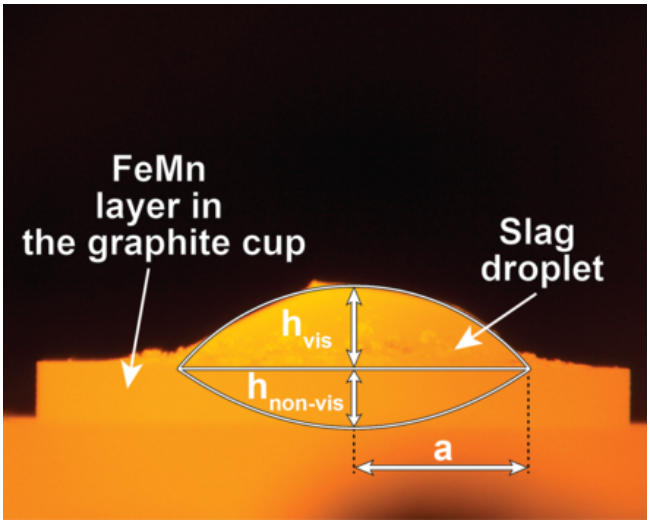

Figure 10: Slag droplet on top of FeMn layer in experiments: a is the base radius of the spherical cap, h_{vis} and $h_{non-vis}$ are the height of the spherical cap above and below the interface, respectively.

4. Calculate the visible volume of the slag droplet, V_{vis}^{slag}:

$$V_{vis}^{slag} = \frac{1}{6}\pi h_{vis}^{exp}\left(3(a^{exp})^2 + (h_{vis}^{exp})^2\right). \tag{15}$$

5. Calculate the non-visible volume of the slag droplet, $V_{non-vis}^{slag}$:

$$V_{non-vis}^{slag} = V_{total}^{slag} - V_{vis}^{slag}. \tag{16}$$

6. Determine the height of the spherical cap below the interface in *meters*, $h_{non-vis}^{exp}$. In this study, a MATLAB script has been developed, allowing to solve the equation for the volume of a spherical cap (eq. 17) and calculate $h_{non-vis}^{exp}$, given that a, h_{vis}^{exp}, $V_{non-vis}^{slag}$ are known.

$$V_{non-vis}^{slag} = \frac{1}{6}\pi h_{non-vis}^{exp}\left(3(a^{exp})^2 + (h_{non-vis}^{exp})^2\right). \tag{17}$$

7. Calculate the non-visible height of the slag droplet in %:

$$h_{non-vis}^{exp}(\%) = \frac{h_{non-vis}^{exp}}{h_{non-vis}^{exp} + h_{vis}^{exp}} \cdot 100. \tag{18}$$

B. Procedure for slag droplets in simulations

1. In simulations, the height of slag droplets both below and above the interface can be obtained directly from measuring distances as shown in Fig. 11.

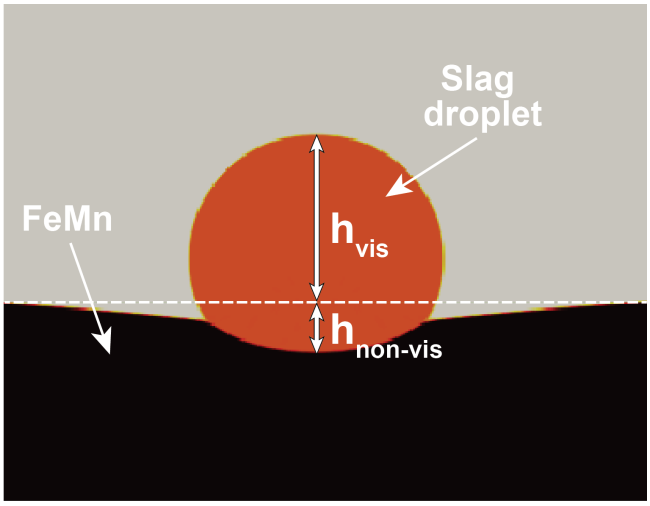

Figure 11: Slag droplet on top of FeMn bath in simulations.

2. Calculate the non-visible height of the slag droplet in %:

$$h^{sim}_{non-vis}(\%) = \frac{h^{sim}_{non-vis}}{h^{sim}_{non-vis} + h^{sim}_{vis}} \cdot 100. \qquad (19)$$

3. The non-visible height of the slag droplet in simulations obtained from equation *19* is compared with experimental values from equation *18* to find the corresponding non-visible height and thereby also the corresponding interfacial tension, which in the simulations was varied according to a range of expected values.

EXPERIMENTAL CONDITIONS AND NUMERICAL SETTINGS

Experimental conditions

The experimental parameters used in experiments in the sessile drop furnace are shown in Table 2.

Table 2: Experimental conditions in the sessile drop furnace.

Parameter	Value in measurement of	
	Surface tension	Interfacial tension
m_{slag}, g	0,120	≈0,050 - 0,060
m_{FeMn}, g	0,120	≈0,300 - 0,350
Ar flow, NLPM	0,1	0,1
Pressure inside the chamber, Pa	101325	101325
Maximum temperature, K	1723	1623, 1673, 1723
Holding time at maximum temperature, min	5	5, 10, 15
Heating rate to 1473 K, K/min	300	300
Heating rate from 1473 K to maximum temperature, K/min	≈25	≈25

Numerical settings and simulation procedure

Simulations were carried out on an axisymmetric 2D geometry as shown in Fig. 12, where the following boundary conditions were applied:

- Left wall - symmetry.
- Right, top and lower wall - no-slip condition with a fixed flux pressure (P = 0 Pa).

The initial number of cells in the simulations was 5000. In order to increase the resolution at the interfaces (slag-Ar, FeMn-Ar, FeMn-slag), 2D dynamic mesh refinement (CFD Online Discussion Forums, 2018) was applied, which allows increasing the number of cells up to 20000 for the given simulation setup. All simulations were performed on resourses

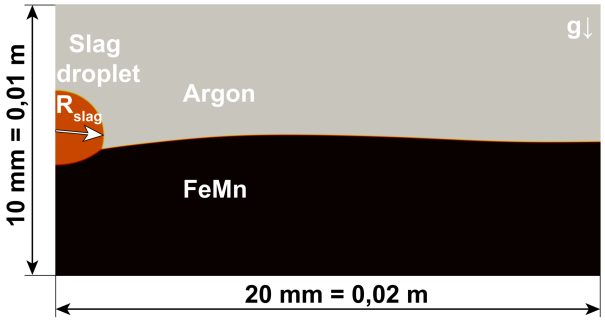

Figure 12: 2D axisymmetric geometry applied in simulations. R_{slag} varies from 0,00147 to 0,00163 m (from 1,47 to 1,63 mm), depending on the weight of a slag droplet, and g is the gravity, acting in y-direction.

provided by the NTNU IDUN computing cluster (Sjalander *et al.*, 2019) using modified settings for damBreak4phase tutorial case (cf. The OpenFOAM Foundation, 2016) with multiphaseInterFoam solver, as shown in Table 3. The presence of so-called spurious currents in VOF simulations results in considerable challenges when aiming to reach a static steady state and therefore low values of under-relaxation factors were applied to reduce spurious currents as it was proposed by Vachaparambil and Einarsrud, 2019. Simulations were aiming to reach steady state conditions corresponding to a droplet at rest. As multiphaseInterFoam is a transient solver, transient simulations with dynamic time stepping from 10^{-5} to 10^{-6} s and the maximum Courant number of 0,25 until 1 s flow time was attained - sufficient to obtain a (quasi) steady state for all simulations considered. The simulations were initialized with a slag droplet with radius from 1,47 to 1,63 mm, depending on the weight of the slag droplet, initially positioned 1,50 mm above the alloy interface.

In addition, a numerical calculation using equation *3* has been carried out to evaluate a relevant range of interfacial tension for the simulations. Values of $\cos\beta$, as illustrated in Fig. 13, are greater than 1 when interfacial tension is smaller than 0,85 N/m. Interfacial tension of 0,85 N/m has therefore been used as the minimum value in simulations, while the maximum interfacial tension is assumed to be identical to surface tension of FeMn - 1,50 N/m.

The physical parameters used in simulations are shown in Table 4.

In order to reduce the effects of spurious currents even more, the viscosity was set to an (artificial) elevated value. Since the steady state is static - the actual value of the viscosity should not impact the final converged result. In order to determine a suitable value for the viscosity - a parametric study was performed, in which the steady state solutions (if found) were compared, according to the values indicated below.

- $10^{-6} \leq \nu_{FeMn} \leq 10^{-2}$ m^2/s.

Table 3: Numerical solution parameters used in the simulation setup.

Solution and algorithm control settings (fvSolution)						
Parameter	**Field**					
	alpha	**pcorr**	**p_rgh**	**p_rghFinal**	**U**	**UFinal**
tolerance	10^{-6}	10^{-8}	10^{-8}	10^{-9}	10^{-6}	10^{-8}
relTor	0	0	0	0	0	0
maxIter	100	-	-	50	-	-
nAlphaSubCycles	2	-	-	-	-	-
nAlphaCorr	2	-	-	-	-	-
MULESCorr	false	-	-	-	-	-
cAlpha	1	-	-	-	-	-
nLimiterIter	3	-	-	-	-	-
smoother	GaussSeidel	-	-	-	-	-
nSweeps	1	-	-	-	-	-
solver	smoothSolver	-	-	-	-	-
relaxationFactors	-	0,3	0,3	0,9	0,3	-

PIMPLE loop	
Parameter	**Value**
nCorrectors	1
nOuterCorrectors	1
momentumPredictor	false

Numerical schemes settings (fvSchemes)	
Time derivatives	**Value**
ddtSchemes	CrankNicolson 0,50

Time and data input/output control settings (controlDict)	
Parameter	**Value**
deltaT	10^{-6}
maxDeltaT	10^{-5}
maxCo	0,25
maxAlphaCo	0,25

- $10^{-5} \leq \nu_{slag} \leq 10^{-3}$ m^2/s.
- $10^{-5} \leq \nu_{Ar} \leq 10^{-3}$ m^2/s.

In addition, a parametric study of the mesh resolution, quality of the dynamic mesh refinement (DMR) and geometry size has been carried out to determine the most appropriate parameters to be used in simulations without affecting the results and changing the convergence time significantly. For all simulations in the parametric study, $\gamma_{slag-Ar}$, $\gamma_{FeMn-Ar}$ and $\gamma_{FeMn-slag}$ were 0,70, 1,00 and 0,70 N/m, respectively.

RESULTS AND DISCUSSION

A. Surface tension of FeMn alloy and slag

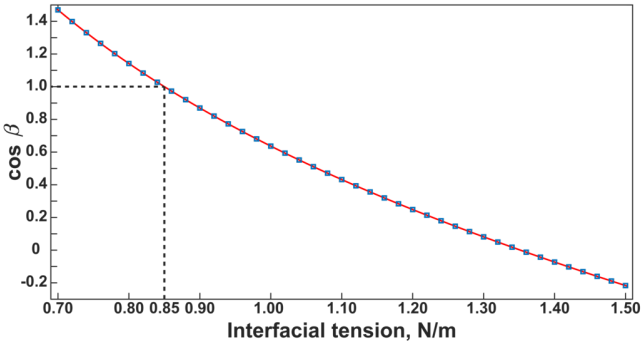

Figure 13: Values of cos β calculated by equation *3*.

Table 4: Physical parameters applied in simulations.

Parameter	**Value**
ρ_{slag}, kg/m^3	3300*
ρ_{FeMn}, kg/m^3	5612*
ρ_{Ar}, kg/m^3	1,66
ν_{slag}, m^2/s	varied
ν_{FeMn}, m^2/s	varied
ν_{Ar}, m^2/s	varied
$\gamma_{slag-Ar}$, N/m	0,65
$\gamma_{FeMn-Ar}$, N/m	1,50
$\gamma_{FeMn-slag}$, N/m	0,85 - 1,50

* Density of slag and FeMn alloy in molten state (Muller *et al.*, 2015)

The values surface tension of FeMn alloy and slag, obtained after the experimental measurement, are shown in Fig. 14. Surface tension of FeMn alloy was found to be 1,50 ± 0,05 N/m, while surface tension of slag was considerably lower (0,65 ± 0,01 N/m). From the confidence intervals, it is evident that the LBADSA methodology, which was applied for the measurement of surface tension of FeMn has higher deviation (±0,05 N/m), that the ellipsoidal solution of the Young-Laplace equation, where the confidence interval for surface tension of slag was ±0,01 N/m.

B. Parametric study: influence of viscosity

For simulations with $\nu_{FeMn} \leq 10^{-6}$ m^2/s, the alloy interface failed to stabilize as indicated in Fig. 15. For values of $10^{-4} \leq \nu_{FeMn} \leq 10^{-2}$ m^2/s, the interface was stable, also for a wide range of viscosities for the remaining phases; $10^{-4} \leq \nu_{slag} \leq 10^{-5}$ m^2/s and $10^{-3} \leq \nu_{Ar} \leq 10^{-5}$ m^2/s, indicated in Fig. 16. Increasing the viscosity further led to unphysical numerical artifacts.

From the parametric study, it was concluded to choose $\nu_{FeMn} = 10^{-4}$ m^2/s, $\nu_{slag} = 10^{-5}$ m^2/s and $\nu_{Ar} = 10^{-5}$ m^2/s. The kinematic viscosity of FeMn differs from the real kinematic viscosity of FeMn, which is usually in the order of 10^{-6} m^2/s; however, the assumed kinematic viscosity of FeMn should not influence the steady state of the simulations as discussed earlier.

C. Parametric study: influence of mesh resolution and geometry size

Studied settings of DMR and mesh resolution, total number

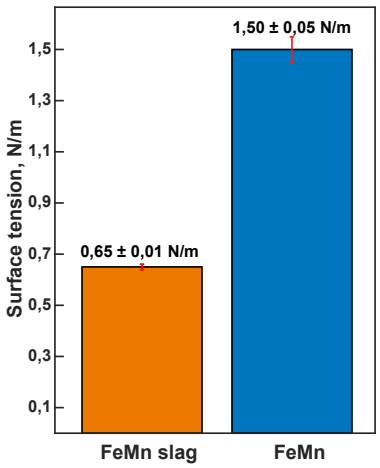

Figure 14: Surface tension of FeMn alloy and slag measured experimentally in the sessile drop furnace. Red lines on top of bars are 95 % confidence intervals.

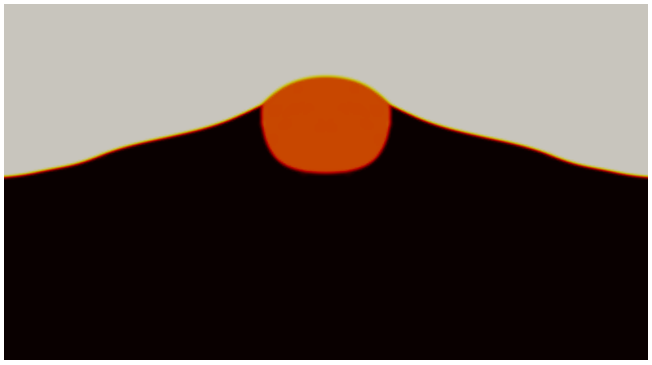

Figure 15: Surface instabilities induced by spurious currents.

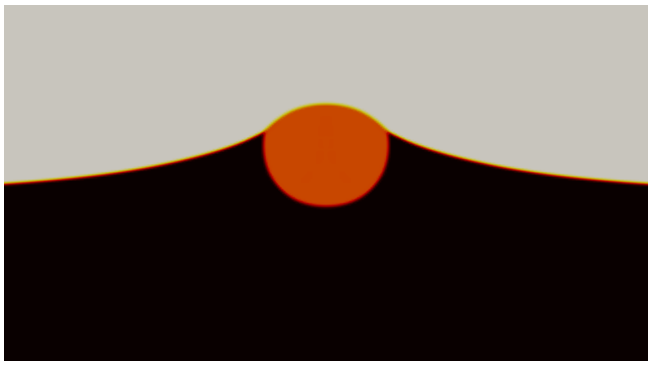

Figure 16: The simulation results for the kinematic viscosity: $\nu_{FeMn} = 10^{-4}$ m^2/s, $\nu_{slag} = 10^{-4}$-10^{-5} m^2/s, $\nu_{Ar} = 10^{-3}$-10^{-5} m^2/s.

of cells before and after DMR as well as maximum time step and convergence time are presented in Table 5. In addition, the influence of geometry size has been studied with the parameters as shown in Table 6. Since the non-visible height of the slag droplet is crucial for obtaining the interfacial tension based on the inverse modelling strategy, it has been applied for comparing the steady state in various simulations.

The non-visible height obtained at different time steps in tests of different mesh resolution and DMR quality is shown in Fig. 17. In test A1 and A2, the slag droplet has reached a steady state as represented in Fig. 18, while the convergence time increases with increasing the quality of DMR as well as the total number of mesh cells after DMR increases up to 2,0 and 3,6 times for low (A1) and average (A2) quality of DMR, respectively. On the contrary, test A3 with the highest quality of DMR and test A5 with the highest number of cells after DMR, have instabilities in achieving the steady state, which leads to higher values of the average non-visible height. Similarly to tests A1 and A2, the increasing of mesh resolution in test A4 does not have any influence on the simulation results, however, the convergence time increases to 24784 s. For the proposed simulation setup, the settings from test A2 with average quality of DMR has been chosen as optimal since it requires slightly higher convergence time compared to test A1 with low quality.

The influence of geometry size in x- and y-direction on the non-visible height of the slag droplet is demonstrated in Fig. 19. Tests B2-B5 have shown similar steady results with relatively close values of the average non-visible height, while test B1 has instabilities at the FeMn-Ar interface, resulting in the average non-visible height two times higher compared to other simulations. Test B2 has been chosen as optimal since it requires the lowest convergence time compared to tests B3-B5 with higher geometry size.

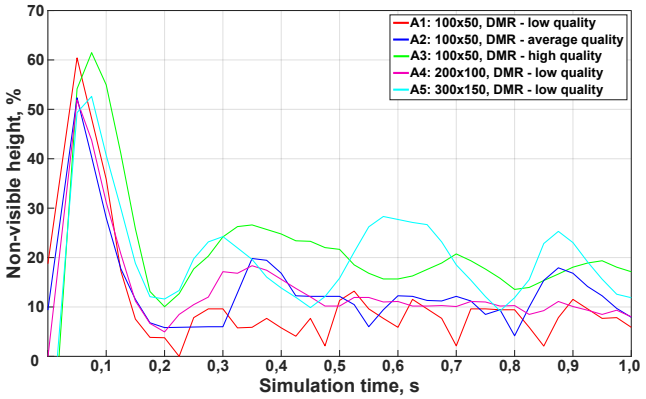

Figure 17: Effect of mesh resolution and DMR quality on the non-visible height of slag droplet in the parametric study. The average non-visible height in percent at the steady state (after 0,2 s of simulation time) for each test is: A1 - 7,4; A2 - 11,2; A3 - 18,9; A4 - 11,2; A5 - 18,4.

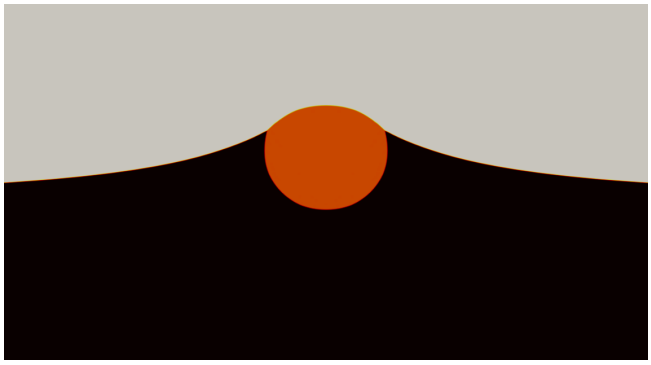

Figure 18: The steady state of slag droplet reached in simulations in the parametric study.

D. Interfacial tension between FeMn alloy and slag

Fig. 20 shows the simulation matrix obtained after performing simulations with various values of interfacial tension and parameters as shown in Table 4, with viscosities and resolution as determined in previous sections. The corresponding non-visible height to the values of interfacial tension from 0,85 to 1,50 N/m is illustrated in Fig. 21. The results demon-

Table 5: Settings for mesh resolution and DMR quality used in the parametric study.

Mesh	DMR quality	Mesh resolution, mm^2	Initial total number of cells	Total number of cells after DMR	Maximum time step, s	Convergence time, s
A1	Low	0,200 x 0,200	5000	10000	10^{-5}	8541
A2	Average	0,200 x 0,200	5000	18000	10^{-5}	14009
A3	High	0,200 x 0,200	5000	44000	10^{-5}	52366
A4	Low	0,100 x 0,100	20000	31800	10^{-5}	24784
A5	Low	0,066 x 0,066	45000	66500	10^{-5}	64886

Table 6: Geometry size used in the parametric study.

Mesh	DMR quality	Mesh resolution, mm^2	Geometry size in x-direction, mm	Geometry size in y-direction, mm	Surface area of the geometry, mm^2	Maximum time step, s	Convergence time, s
B1	Low	0,200 x 0,200	10	10	100	10^{-5}	5013
B2	Low	0,200 x 0,200	20	10	200	10^{-5}	8375
B3	Low	0,200 x 0,200	20	20	400	10^{-5}	11189
B4	Low	0,200 x 0,200	20	40	800	10^{-5}	21703
B5	Low	0,200 x 0,200	50	10	500	10^{-5}	17822

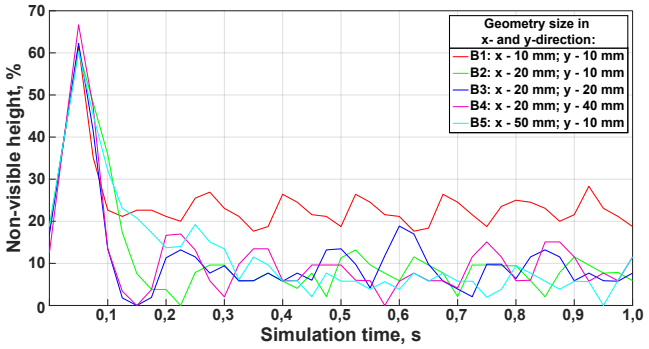

Figure 19: Effect of the geometry size on the non-visible height of slag droplet in the parametric study. The average non-visible height in percent at the steady state (after 0,2 s of simulation time) for each test is: B1 - 22,3; B2 - 7,4; B3 - 9,0; B4 - 8,8; B5 - 7,4.

strate that the slag droplet remains above the interface at relatively high values of interfacial tension (≈1,20 - 1,50 N/m), which promotes better separation of FeMn alloy and slag and therefore less metal losses. The slag droplet begins to sink down below the interface at intermediate interfacial tension (≈0,85 - 1,15 N/m), contributing to emulsification of FeMn and slag.

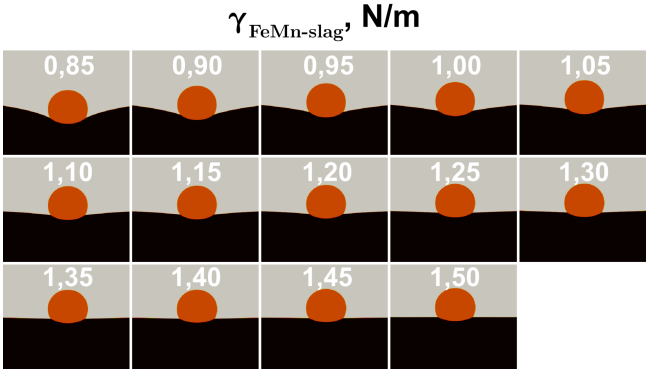

Figure 20: The simulations results, depending on interfacial tension between FeMn alloy and slag from 0,85 to 1,50 N/m.

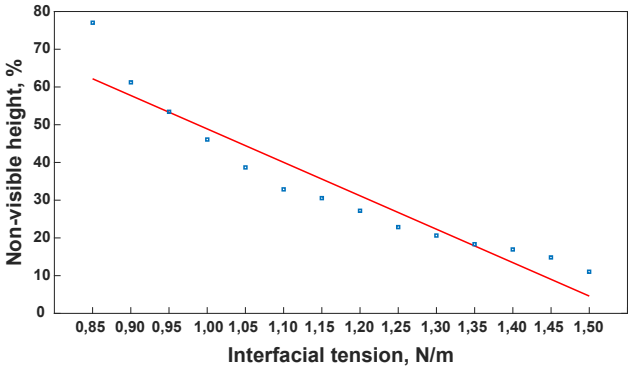

Figure 21: Effect of interfacial tension on the non-visible height in the simulations.

The simulations shown in Fig. 20 were compared to the non-visible part of slag droplets from corresponding experiments, from which the interfacial tension could be estimated under various conditions. Figure 22 shows a comparison of the non-visible surface to that obtained under simulations under similar conditions. The estimated interfacial tension between FeMn alloy and slag at different temperatures and holding time is presented in Fig. 23 and Fig. 24, respectively. According to Fig. 23, the interfacial tension gradually decreases from 1,50 ± 0,05 N/m to 1,15 ± 0,04 N/m when temperature increases. Fig. 24 shows that the holding time of 5 and 10 min has no effect on the interfacial tension; however, interfacial tension slightly decreases to 1,25 N/m when the holding time is 15 min.

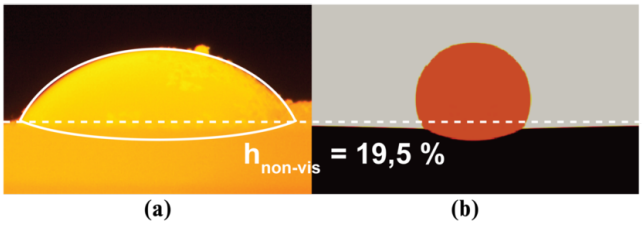

Figure 22: Comparison of the slag surface obtained experimentally at 1673 K (a) and in simulations (b), corresponding to interfacial tension of 1,30 N/m.

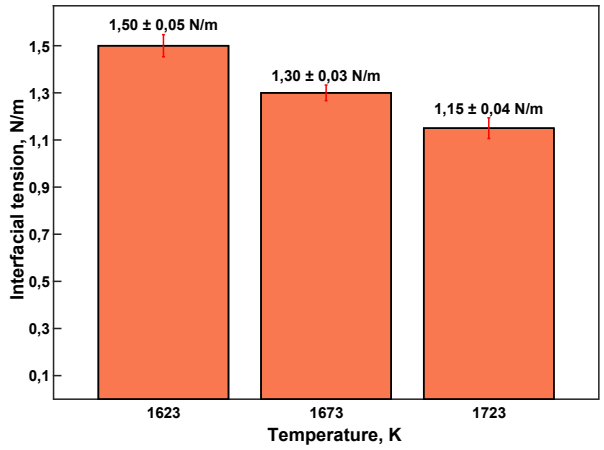

Figure 23: Effect of the temperature on interfacial tension between FeMn alloy and slag. Red lines on top of bars are 95 % confidence intervals.

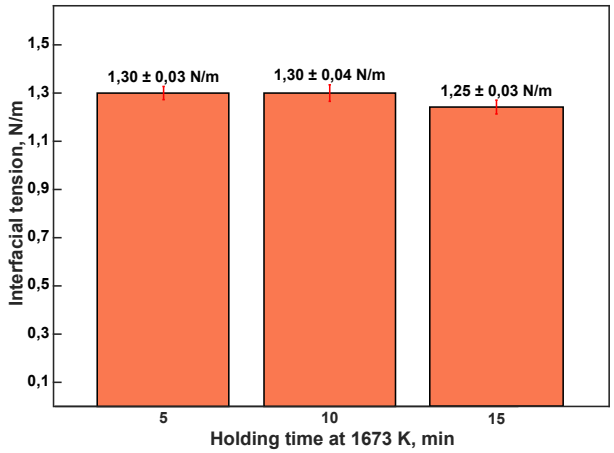

Figure 24: Effect of the holding time on interfacial tension between FeMn alloy and slag at constant temperature. Red lines on top of bars are 95 % confidence intervals.

F. Previous research on surface tension of FeMn alloy and slag

Lee *et al.*, 2011 have reported that the surface tension of FeMn alloys without carbon decreases with increasing the Mn content - from ≈1,90 N/m for a pure Fe-system to ≈1,00 N/m for a pure Mn-system. According to their data, the corresponding value of surface tension is 1,10 N/m for the composition used in this study, assuming that no carbon is present in FeMn alloy (≈84 wt. % Mn, ≈16 wt. % Fe). However, they have not studied the influence of carbon on the Fe-Mn system, which can explain the difference in the surface tension of FeMn alloy - 1,10 N/m in Lee *et al.*, 2011 compared to 1,50 N/m in the present work for high-carbon saturated FeMn alloy. Xin *et al.*, 2019 developed a numerical model for calculation of the surface tension of molten slags which predicts that molten slags generally have surface tension in the range from 0,30 to 0,70 N/m, depending on the composition, again corresponding well to that identified in the current work.

While there to our best knowledge is no data for interfacial tension between FeMn alloy and slag, Park *et al.*, 2009 have reported interfacial tension between molten iron and CaO-SiO_2-MgO-Al_2O_3-FeO slag between 0,72 and 1,44 N/m, depending on slag composition and oxygen content in iron. Surface tension of FeMn slag (0,65 N/m) and interfacial tension between FeMn alloy and FeMn slag (1,15-1,50 N/m), again in the range of that found in the current work.

SUMMARY AND CONCLUSIONS

The current paper presents a method in which images from a sessile drop furnace are combined with multiphase simulations in order to determine material properties which otherwise are not easily accessible. The method is demonstrated for a FeMn-slag system with constant composition.

The proposed method estimates interfacial tensions of 1,50 ± 0,05 N/m, 1,30 ± 0,03 N/m and 1,15 ± 0,04 N/m at temperatures of 1623, 1673 and 1723 K, respectively. Furthermore, it has been found that changing the holding times from 5 to 15 minutes does not affect the interfacial tension significantly. Surface active elements, such as S, can have a considerable impact on interfacial tension. Although it is not addressed in the current work, experiments considering such effects have been carried out recently, and will be published in the near future (Bublik *et al.*, 2021).

The methodology developed here is demonstrated only for FeMn; however, it is expected that it could also be applied for other processes, i.e. metal refining and for other metals, for instance, SiMn, FeSi, Si and Fe. Future work will explore these possibilities as well as the influence of slag composition for the FeMn system.

REFERENCES

ANDERSSON, P. (2010). "Tutorial multiphaseInterFoam". `http://www.tfd.chalmers.se/~hani/kurser/OS_CFD_2010/patrikAndersson/patrikAnderssonReport.pdf`. Accessed: 24.08.2020.

BERBEROVIC, E., VAN HINSBERG, N.P., JAKIRLIC, S., ROISMAN, I.V. and TROPEA, C. (2009). "Drop impact onto a liquid layer of finite thickness: Dynamics of the cavity evolution". *Phys. Rev. E*, **79**, 036306.

BUBLIK, S., BAO, S., TANGSTAD, M. and EINARSRUD, K.E. (2019). "Slag-metal interactions in the FeMn tapping process: Interfacial properties and wetting". *Proceedings of the Liquid Metal Processing & Casting Conference 2019*. Birmingham, UK.

BUBLIK, S., BAO, S., TANGSTAD, M. and EINARSRUD, K.E. (2021). "Influence of sulphur on the interfacial behaviour between FeMn alloy-slag and SiMn alloy-slag". To be presented at MOLTEN 2021.

CFD Online Discussion Forums (2018). "Main Forum". `https://www.cfd-online.com/Forums/openfoam-community-contributions/118870-2d-adaptive-mesh-refinement-2.html#post703369/`. Accessed: 24.08.2020.

CLIFT, R., GRACE, J. and WEBER, M. (1978). *Bubbles, Drops, and Particles*. Academic Press.

DAMIAN, S.M. (2012). "Description and utilization of interFoam multiphase solver". *International Center for Computational Methods in Engineering*.

HERNANDEZ-BALTAZAR, E. and GRACIA-FADRIQUE, J. (2005). "Elliptic solution to the Young–Laplace differential equation". *Journal of Colloid and Interface Science*, **287(1)**, 213 – 216.

HIRT, C. and NICHOLS, B. (1981). "Volume of fluid (VOF) method for the dynamics of free boundaries". *Journal of Computational Physics*, **39(1)**, 201 – 225.

HOLAPPA, L. (2013). "Chapter 2 - Basics of Ferroalloys". M. Gasik (ed.), *Handbook of Ferroalloys*. Butterworth-Heinemann, Oxford.

JAKOBSSON, A., SICHEN, D., SEETHARAMAN, S. and NURNI, V. (2000). "Interfacial phenomena in some slag-metal reactions". *Metallurgical and Materials Transactions B*, **31**, 973–980.

KIM, H., KIM, J. and SASAKI, Y. (2010). "The role of molten slag in iron melting process for the direct contact carburization: Wetting and separation". *ISIJ international*, **50**, 1099–1106.

LEE, J.J.E. (2016). "Droplet formation mechanisms in metallurgical processes".

LEE, J., SHIN, M. *et al.* (2011). "Density and surface tension of liquid Fe-Mn alloys". *Metallurgical and Materials Transactions B*, **42(3)**, 546–549.

LI, Z., ZEZE, M. and MUKAI, K. (2003). "Surface tension and wettability of liquid Fe-16 mass%Cr-S alloy with alumina". *Materials Transactions*, **44(10)**, 2108–2113.

MULLER, J., ZIETSMAN, J. and PISTORIUS, P. (2015). "Modeling of manganese ferroalloy slag properties and flow during tapping". *Metallurgical and Materials Transactions B*, **46**.

OOI, H., NOZAKI, T. and YOSHII, H. (1974). "The effect of chemical reactions on the interfacial tension between iron and CaO-SiO_2-Al_2O_3 slag". *Transactions of the Iron and Steel Institute of Japan*, **14(1)**, 9–16.

PARK, S.C., GAYE, H. and LEE, H.G. (2009). "Interfacial tension between molten iron and CaO–SiO_2–MgO–Al_2O_3–FeO slag system". *Ironmaking & Steelmaking*, **36(1)**, 3–11.

ROWLINSON, J. and WIDOM, B. (2002). *Molecular Theory of Capillarity*. Dover books on chemistry. Dover Publications.

RUEDEN, C.T., SCHINDELIN, J., HINER, M.C., DEZONIA, B.E., WALTER, A.E., ARENA, E.T. and ELICEIRI, K.W. (2017). "ImageJ2: ImageJ for the next generation of scientific image data". *BMC bioinformatics*, **18(1)**, 529.

SARIDIKMEN, H., KUCUKKARAGOZ, C.S. and ERIC, R.H. (2007). "Sulphur behaviour in ferromanganese smelting".

SJALANDER, M., JAHRE, M., TUFTE, G. and REISSMANN, N. (2019). "EPIC: An energy-efficient, high-performance GPGPU computing research infrastructure".

STALDER, A.F., MELCHIOR, T., MULLER, M., SAGE, D., BLU, T. and UNSER, M. (2010). "Low-bond axisymmetric drop shape analysis for surface tension and contact angle measurements of sessile drops". *Colloids and Surfaces A: Physicochemical and Engineering Aspects*, **364(1)**, 72 – 81.

TANGSTAD, M. (2013). *Handbook of Ferroalloys: Chapter 7. Manganese Ferroalloys Technology*. Elsevier Science.

The OpenFOAM Foundation (2016). "OpenFOAM v6 User Guide". `https://cfd.direct/openfoam/user-guide-v6/`. Accessed: 24.08.2020.

VACHAPARAMBIL, K.J. and EINARSRUD, K.E. (2019). "Comparison of surface tension models for the volume of fluid method". *Processes*, **7(8)**, 542.

WELLER, H.G., TABOR, G., JASAK, H. and FUREBY, C. (1998). "A tensorial approach to computational continuum mechanics using object-oriented techniques". *Computers in Physics*, **12(6)**, 620–631.

XIN, J., WANG, N., CHEN, M. and GAN, L. (2019). "Surface tension calculation of molten slag in SiO_2–Al_2O_3–CaO–MgO systems based on a statistical modelling approach". *ISIJ International*, **59(5)**, 759–767.